ORIGINAL ARTICLE

Analysis of capecitabine metabolites in conjunction with digital autoradiography in a murine model of pancreatic cancer suggests extensive drug penetration through the tumor

James Russell[1] | Louise Fanchon[1] | Hanan Alwaseem[2] | Henrik Molina[2] |
Isabella O'Donoghue[1] | Amber Bahr[3] | Elisa de Stanchina[3] |
Nagavarakishore Pillarsetty[4] | John L. Humm[1]

[1]Department of Medical Physics, Memorial Sloan Kettering Cancer Center, New York, New York, USA

[2]The Proteomics Resource Center, The Rockefeller University, New York, New York, USA

[3]Anti-Tumor Assessment Core Facility, Memorial Sloan Kettering Cancer Center, New York, New York, USA

[4]Department of Radiology, Memorial Sloan Kettering Cancer Center, New York, New York, USA

Correspondence
James Russell, Department of Medical Physics, Memorial Sloan Kettering Cancer Center, 1275 York Avenue, New York, NY 10021, USA.
Email: russellj@mskcc.org

Abstract

Previously published digital autoradiography of ^{3}H-labeled capecitabine reveals a near-uniform distribution of activity throughout a murine pancreatic model. This is in contrast both to ^{14}C-labeled gemcitabine, and established expectations, as the dense stroma of pancreatic cancer is understood to inhibit drug penetration. Capecitabine is a pro-drug for 5 FU. The positioning of the radiolabel on capecitabine leaves open the possibility that much of the autoradiographic signal is generated by nontoxic compounds. Studies were performed on tumors derived via organoid culture from a murine KPC tumor. As before, we performed autoradiography comparing ^{3}H capecitabine to the gemcitabine analog ^{18}F-FAC. The metabolism of capecitabine in this model was studied through LC–MS of tumor tissue. The autoradiographs confirmed that the ^{3}H label from capecitabine was much more uniformly distributed through the tumor than the ^{18}F from the gemcitabine analog. LC–MS revealed that approximately 75% of the molar mass of capecitabine had been converted into 5 FU or pre-5 FU compounds. The remainder had been converted into nontoxic species. Therapeutically relevant capecitabine metabolites achieve a relatively even distribution in this pancreatic cancer model, in contrast to the gemcitabine analog ^{18}F-FAC. In a human xenograft model, (BxPC3), the ^{3}H label from capecitabine was also uniformly spread across the tumor autoradiographs. However, at 2 h post-administration the metabolism of capecitabine had proceeded further and the bulk of the agent was in the form of nontoxic species.

KEYWORDS
autoradiography, capecitabine, gemcitabine, LC–MS, pancreatic cancer

---

1 | INTRODUCTION

Dense stroma is a hallmark of pancreatic cancer, and is recognized as a serious barrier to drug penetration into the tumor mass.[1,2] This microenvironment is well recapitulated in tumors arising in genetically engineered mice[3] (the KPC model; K-ras and p53 mutations are expressed in pancreatic cells, leading to spontaneous tumor formation). In this model, poor penetration of both gemcitabine and doxorubicin have been demonstrated.[4] Furthermore, in this model interventions that alleviate stromal burden, notably hedgehog inhibitors and hyaluronidase treatment, showed considerable promise as therapy enhancers.[3,4] However, these promising results did not translate to clinical benefit.[5,6]

Given the concerns over drug access, it is surprising to note the success of the hypoxia tracers pimonidazole[7] and ^{18}F-FAZA[8] in identifying hypoxic tissue in clinical samples of pancreatic cancer; hypoxic tissue being remote from open blood vessels must represent the least accessible tumor regions. An obvious explanation would be that while the tracers may diffuse slowly into the tumor mass, their chemistry prevents entrapment in oxygenated regions. Thus, it may be that difficulties with drug diffusion are not simply explained by slow drug penetration, but also require consideration of how rapidly the agent is being bound by adjacent tumor cells.

In this context, we recently published observations showing that when autoradiography of radiolabeled drug was employed, gemcitabine and 5 FU—both mainstays of pancreatic chemotherapy—were very nonuniformly distributed through tumor mass in KPC-derived tumors.[9] However, capecitabine, which is a 5 FU prodrug, yielded autoradiograph images that were essentially uniform across the tumor area. A significant caveat of such results is that as the autoradiographs report on the radiolabel, and considering capecitabine's extensive metabolic fates, it is challenging to characterize whether signal originates from active or inactive metabolites. Indeed, the position of the capecitabine radiolabel (^{3}H at C6 on the pyrimidine ring), leads to it being retained in all the reported metabolites.[10]

In order to understand the fate of capecitabine and its metabolites in this model, we performed bulk analysis of tumors using LC–MS. The main breakdown products of capecitabine are illustrated in Figure 1. They can be functionally classified into three groups: 5 FU and its precursors; inactive metabolites of 5 FU; and phosphorylated cytotoxic metabolites of 5 FU. (The chemistry of 5 FU is well established; for one review, see Peters and van Groenigen[11]). Although there is no way to spatially map each metabolite on tumor sections, we reasoned that a preponderance of one group of compounds in bulk analysis would help inform our interpretation of the autoradiographic data.

Finally, we chose to conduct our studies in KPC-derived tumors, supplemented with information from the human pancreatic BxPC-3 model, as published studies describe both systems as being capecitabine responsive.[12,13]
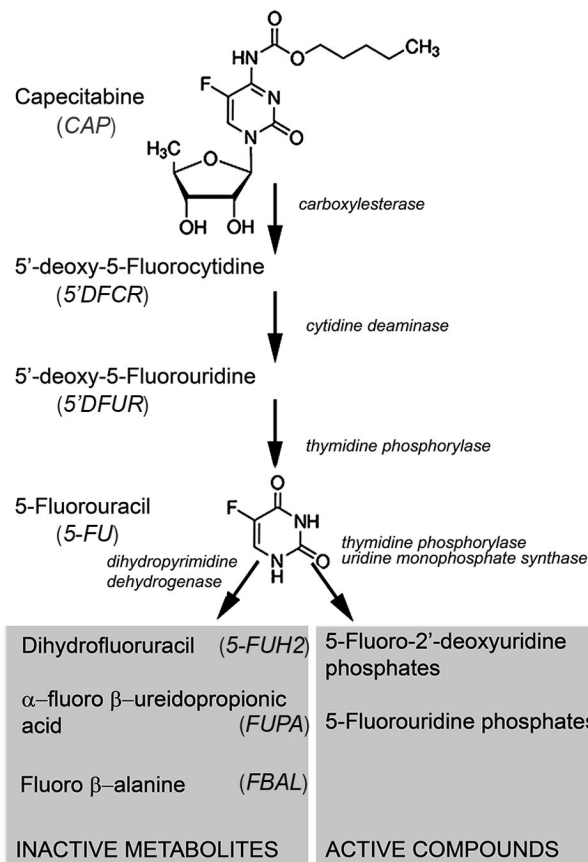

FIGURE 1 A simplified metabolic pathway, showing the activation of capecitabine to 5 FU and its subsequent fates

2 | MATERIALS AND METHODS

2.1 | Tumor models

All experiments described here were performed with the knowledge and express permission of Memorial Sloan Kettering Cancer Center's Institutional Animal Care and Use Committee, and housed in the MSKCC vivarium, an IACUC and AAALAC approved facility. The transplantable tumor model used here has been previously described.[9] An organoid culture derived from a KPC pancreatic tumor was the generous gift of Dr D.A. Tuveson, Cold Spring Harbor Laboratories, NY. A tumor was established from the culture by orthotopic implantation into a C57Bl/6 mouse (Jackson Laboratories) and expanded through serial transplantation. Tumors used in these experiments were in the fourth passage. BxPC3 cells (RRID:CVCL_0186) were obtained from the American Type Culture Collection (ATCC), and injected orthotopically into athymic mice (Jackson Laboratories). Surgeries were performed by the MSKCC core, as previously described.[9,14] The experiments used female mice aged between 7 and 10 weeks at time of implantation. For KPC-derived tumors, experiments were conducted 3–4 weeks after implantation, and for BxPC3 tumors, experiments at 6–8 weeks' post-injection.

2.2 | Autoradiography and image analysis

^{18}F-FAC synthesis was performed as previously described.[15] ^{3}H Capecitabine was purchased from Moravek Biochemicals. Animals were given ^{3}H-capecitabine (925 kBq) by gavage in 5% Gum Arabic, 40 mM citrate buffer, pH 6.0, 0.2 ml, and ^{18}F-FAC (2220 kBq) in 0.2 ml saline intraperitoneally. Animals were euthanized 2 h after tracer administration by CO_2 inhalation. Tumors were removed, frozen in OCT and 10 μm sections were cut. Five adjacent sections were cut at 2–3 depths per tumor, separated by at least 500 μm. For image registration, slides were marked with nail varnish containing ^{18}F and ^{14}C (740 and 7.4 Bq/μl, respectively) as well as crystal violet, such that the markers (3/slide) were visible on autoradiographs and microscopic images. ^{18}F images were collected by exposing slides to BAS-IP2025 plates for 2 h (one ^{18}F half-life). Twenty-four hours later, the ^{3}H exposure was initiated on BAS-TR2025 (FujiFilm). Tritium exposures were for 2 months at −80°C.

Images were collected on a Typhoon FLA7000 scanner (GE Healthcare). Upon completion of scanning, a brightfield image of the slide, showing tumor section and autoradiograph markers was collected using an Olympus BX60 microscope with Microsuite Biological Imaging software (Olympus America). The markers were then removed from the slide, which was stained with hematoxylin and eosin (Vector Laboratories), and imaged as before. The H&E image was matched to the brightfield image, based on tumor outline, and the autoradiographs were matched to the image based on the markers. To reduce noise in the ^{3}H images, adjacent sections were registered in ImageJ with the *StackReg* plugin, and a median image obtained, as described previously.[9] The H&E images were used to exclude nonviable tissue from the autoradiographs; histograms of pixel intensity values were constructed, comparing ^{18}F-FAC to ^{3}H capecitabine.

2.3 | Liquid chromatography–mass spectroscopy

Tumor-bearing animals were gavaged with nonlabeled capecitabine (Sigma-Aldrich, 250 mg/kg, in Gum Arabic as above). Animals were euthanized 2 h post-dosing, and the tumors removed. Tumor fragments (25 mg) were homogenized on ice into 0.2 ml LC–MS grade water (EMD Millipore) followed by extraction with 0.96 ml of HPLC grade chloroform/methanol (2:1) (Fisher Scientific). The samples were vortexed vigorously for 10 min at 4°C, centrifuged for 10 min (9000 *g*, 4°C) and the methanol/water layer was transferred into a pre-chilled Eppendorf tube. The samples were snap-frozen in liquid nitrogen and dried using a SpeedVac. The dried samples were reconstituted in 50 μl of 50% LC–MS grade acetonitrile (Fisher Scientific), vortexed for 30 s, centrifuged for 1 h (13 200 rpm, 4°C) and 2 μl of each biological sample was injected onto the LC–MS system in a randomized order. A quality control mixture was prepared by pooling 12 μl of each treated sample into one Eppendorf tube. This pool mixture was injected every 4 h to monitor instrument performance.

Capecitabine metabolites were separated on a ZIC-pHILIC 150 × 2.1 mm (5-μm particle size) column (EMD Millipore) connected to a Thermo Vanquish ultrahigh-pressure liquid chromatography (UPLC) system and mass spectrometric analysis was performed using a Q Exactive benchtop orbitrap mass spectrometer equipped with a heated electrospray ionization (HESI) probe as described previously.[16] Skyline Daily (version 21.0.9.118) was used to process the raw data with a maximum mass and retention time tolerance set to 2 ppm and 6 s, respectively, referencing a library of capecitabine metabolite standards. Quantitation of capecitabine and its metabolites was achieved using linear regression analysis. Calibration curves were prepared using untreated tumor, processed as described above, with known amounts of capecitabine metabolites added to the homogenate (prior to extraction). The reference standards used were: fluorodeoxyuridine triphosphate, fluorouridine triphosphate, (Sierra Bioresearch); 5,6-dihydro-5-fluorouracil, 5' deoxy-5-fluorocytidine (Cedarlane Laboratories); 5' deoxy-5-fluorouridine, fluoro-β-alanine, 5-fluoro-2'-deoxyuridine monophosphate, 5-fluorouracil (Sigma-Aldrich); α-fluoro-β ureidopropionic acid (ChemSpace).

Stock solutions of capecitabine and its metabolites were individually prepared. 5' deoxy-5-fluorocytidine, 5' deoxy-5-fluorouridine, and capecitabine were dissolved in 80% LC–MS grade methanol (Fisher Scientific). 5-fluorouracil and 5,6-dihydro-5-fluorouracil were dissolved in dimethylformamide. Fluoro-β-alanine and 5-fluoro-2'-deoxyuridine monophosphate were dissolved in LC–MS grade water. α-fluoro-β ureidopropionic acid was dissolved in 20 mM ammonium carbonate (pH 9.3). The stock solutions were diluted 10-fold into 80% LC–MS grade methanol followed by a second 10-fold dilution into 80% LC–MS grade methanol to prepare the working solutions at the following concentrations: 1–32 μmol/L for 5-fluorouracil; 0.5–64 μmol/L for fluoro-β-alanine; 0.5–16 μmol/L for 5' deoxy-5-fluorocytidine; 0.25–32 μmol/L for 5,6-dihydro-5-fluorouracil; 0.125–16 μmol/L for 5' deoxy-5-fluorouridine and α-fluoro-β ureidopropionic acid; 32–512 nmol/L for capecitabine. Calibration curves were not prepared for the nucleotide standards as they were not detected in the treated tumor samples. Fifty microliters of the working solution was incubated with 0.2 ml of clarified untreated tumor and processed as described above. The calibration curves were obtained by plotting the peak area of each metabolite against the known metabolite concentration. A linear trendline fitted using Microsoft Excel with the intercept set to 0, yielded r-squared values >0.99.

Metabolite identity was confirmed via parallel reaction monitoring (PRM) of the pool sample. The PRM method contained two scan events starting with a full scan followed by targeted MS/MS for precursor ions scheduled in an inclusion list. The full MS scan was acquired with 70 000 resolution, 1×10^6 automatic gain control (AGC) target, 80-ms max injection time, and a scan range of 55–825 *m/z*. The targeted MS/MS scans were acquired at a resolution of 17 500, 2×10^5 AGC target, 100-ms max injection time, 1.6-Da isolation width, and stepwise normalized collision energy (NCE) of 20, 30, and 40 units. The inclusion list was as follows: 5,6-dihydro-5-fluorouracil (*m/z* 131.0262 [M-H], 3.5 min), 5' deoxy-5-fluorocytidine (*m/z* 246.0885 [M + H], 5.6 min); 5' deoxy-5-fluorouridine (*m/z* 245.0579

[M-H], 4.4 min); fluoro-β-alanine (m/z 106.0310 [M-H], 12.8 min); 5-fluorouracil (m/z 129.0106 [M-H], 5.2 min); α-fluoro-β ureido-propionic acid (m/z 149.0368 [M-H], 12.7 min); capecitabine (m/z 360.1565 [M + H], 2.5 min).

2.4 | Nomenclature of targets and ligands

Key protein targets and ligands in this article are hyperlinked to corresponding entries in http://www.guidetopharmacology. org, the common portal for data from the IUPHAR/BPS Guide to PHARMACOLOGY,[17] and are permanently archived in the Concise Guide to PHARMACOLOGY 2019/20[18]

3 | RESULTS

Autoradiographic images showing the distribution of [3]H 2 h after injection of labeled capecitabine are shown in Figure 2A. As a comparison, animals were injected with ^{18}F-FAC at the time of capecitabine administration (Figure 2B).[19] FAC is a close analog of gemcitabine, being mono-fluorinated at the 2' position, where gemcitabine is di-fluorinated, and the inter and intratumor distribution of ^{18}F-FAC is highly correlated with gemcitabine.[14,20] (It is necessary to use ^{18}F-FAC as a surrogate for gemcitabine in these studies as the short half-life of ^{18}F makes dual autoradiography possible and it is not chemically possible to generate ^{18}F-labeled gemcitabine.)

For analysis, H&E images were collected (Figure 2C) and these were co-registered to the autoradiographs by means of shared fiduciary markers present on the slide, to exclude necrotic tissue. The homogeneity of both labels is represented by cumulative histograms, obtained from activity in tumor tissue (Figure 2D). Activity is normalized to the median bin: thus, a completely uniform distribution would have all its values as 1 and be represented on the plot as a vertical line. The ^{3}H lines come close to this ideal situation; by contrast, the ^{18}F histograms generally show a tail, indicating the presence of hot spots on the autoradiographs. Furthermore, the lack of agreement between ^{3}H capecitabine and ^{18}F-FAC is visible statistically in the correlation coefficients relating the ^{3}H and ^{18}F pixel values. By combining the tumors presented here with our previous set,[9] the average value for r is −0.16, 95% intervals −0.41 to 0.1 ($n = 4$). By contrast, as reported before, the correlation between ^{14}C gemcitabine and ^{18}F-FAC was highly significant ($r = 0.68$, 95% intervals 0.62 to 0.69, $n = 5$).

The chemical identity of capecitabine metabolites was investigated by LC–MS. As preliminary experiments with tritiated capecitabine and trichloroacetic acid precipitation had found little to no evidence of incorporation into DNA/RNA at 2 h after administration, a low molecular weight screen should fully capture the distribution of capecitabine-derived species at this time point. The LC–MS was unable to detect any of the expected phosphorylated metabolites of capecitabine/5 FU, with all the products being either 5 FU and its precursors, or the noncytotoxic breakdown products. The following
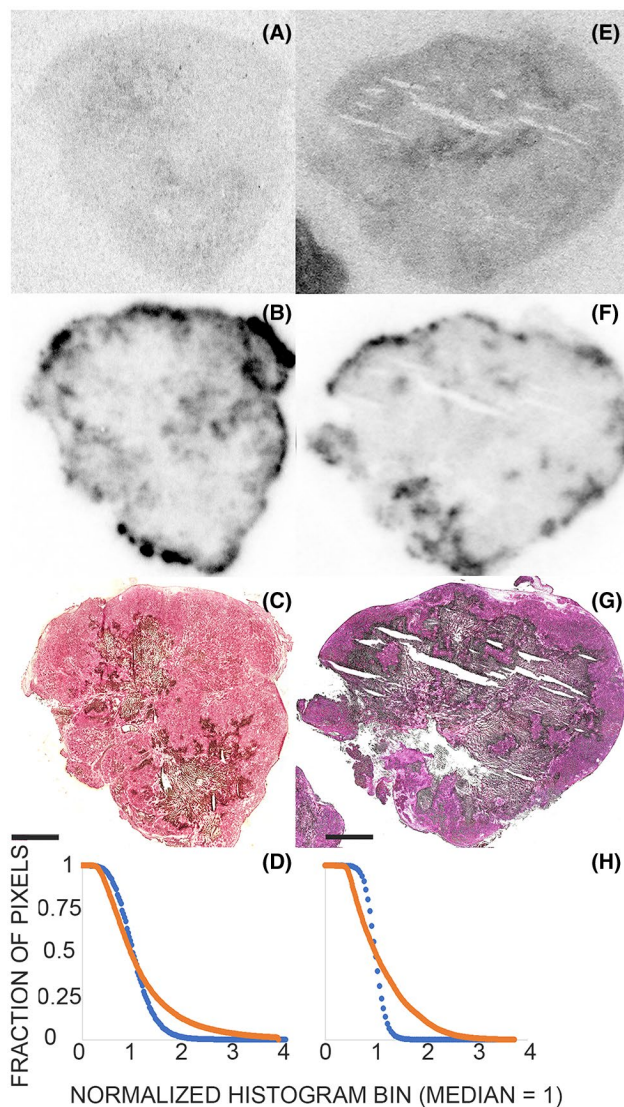
FIGURE 2 Distribution of 3H capecitabine and 18F-FAC in 2 KPC derived tumors. (A,B) 3H autoradiographs (C,D) 18 F autoradiographs (E,F) Hematoxylin & Eosin images; scale bar = 2 mm. (G,H) Cumulative histograms representing the spread of activity in the 3H (blue) and 18F (orange) autoradiographs. Analysis was carried out at a total of 5 depths over 2 tumor sections, all yielding similar histogram plots, i.e. an extended "tail" in the 18F signal, indicative of hotspots, which was not visible in the 3H signal

solvents were tested to optimize the extraction of the phosphorylated metabolites: methanol, methanol/chloroform, ammonium hydroxide/water. However, no conditions yielded measurable phosphorylated product. Therefore, it was concluded that the amount of injected drug that had been phosphorylated at this timepoint was below the limit of detection of the mass spectrometer. As shown in Figure 3, approximately 75% of the drug is in the form of 5 FU or precursors (95% confidence intervals 72%–78%). The summed molar amounts of capecitabine-derived species were approximately 0.029 nanomoles/mg of tissue, or 29 μM, if we treat the weight of tissue as representing the volume of tumor cells.
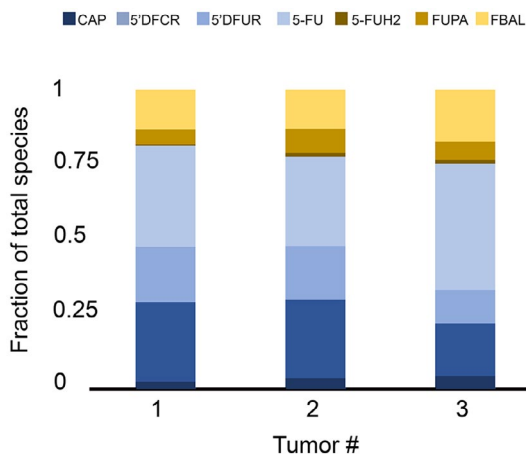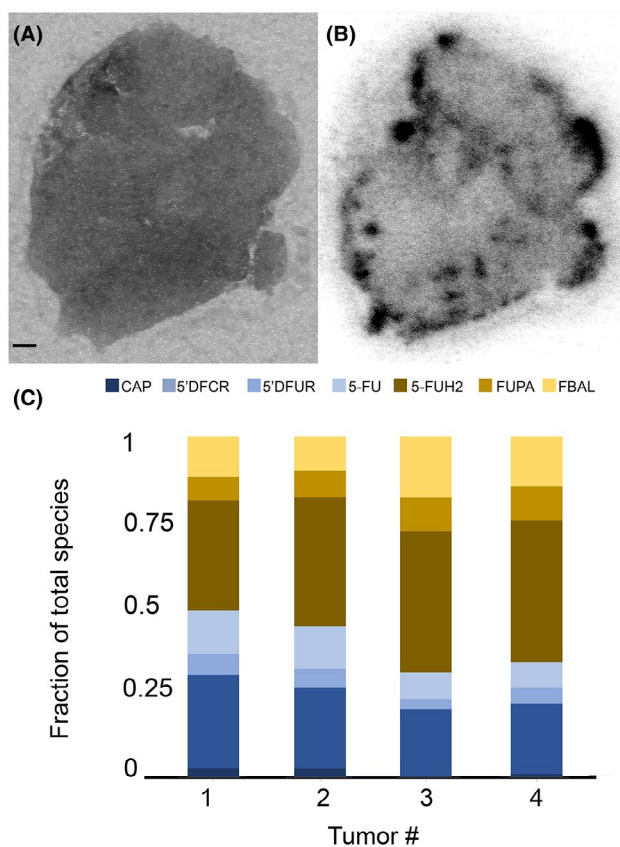
FIGURE 3 The metabolic fate of capecitabine in 3 independent KPC-derived tumors. The pre-active species are represented in shades of blue, ordered as in the metabolic pathway: capecitabine (CAP), 5'-deoxy-5-fluorocytidine (5'DFCR), 5'-deoxy-5-fluorouridine (5'DFUR), 5-fluorouracil (5-FU). The inactive metabolites, are represented in shades of gold, also as ordered as in the metabolic pathway: 5,6 dihydrofluorouracil (5-FUH2), α-fluoro-β-ureidopropionic acid (FUPA), β-fluoroalanine (FBAL). Values are the average of three replicates; 78% of injected drug is in the form of pre-active species, ± 2.5% (SD)

FIGURE 4 Capecitabine uptake and metabolism in orthotopic BxPC3 tumors. Autoradiographs from a representative cryosection section: (A) 3H and (B) 18F-FAC. As the section contained minimal necrosis, the matched Hematoxylin & Eosin image is omitted. Scale bar = 1 mm. (C) The metabolic fate of capecitabine in 4 independent BxPC3 tumors. The pre-active species are represented in shades of blue, ordered as in the metabolic pathway: capecitabine (CAP), 5'-deoxy-5-fluorocytidine (5'DFCR), 5'-deoxy-5-fluorouridine (5'DFUR), 5-fluorouracil (5-FU). The inactive metabolites are represented in shades of gold, also as ordered as in the metabolic pathway: 5,6 dihydrofluorouracil (5-FUH2), α-fluoro-β-ureidopropionic acid (FUPA), β-fluoroalanine (FBAL). Values are the average of three replicates; 40% of injected drug is in the form of pre-active species, ± 7.4% (SD)

Because the rate at which 5 FU is generated from capecitabine will vary from tumor to tumor, we also measured capecitabine metabolites in a separate model: orthotopic BxPC3 xenografts. In a provisional analysis, the autoradiographs also showed an even distribution of capecitabine across the tumor sections. An example is shown in Figure 4A,B. However, these tumors showed a more extensive metabolism of capecitabine (Figure 4C), with a greater accumulation of inactive metabolites by 2 h post-administration. Only 40% of drug was in a potentially active form (95% confidence intervals 32–48%).

4 | DISCUSSION

In our murine tumor model radiolabel from capecitabine was evenly distributed across the tumor sections. By contrast, the gemcitabine analog ^{18}F-FAC was concentrated in hot spots, leaving other areas of the tumor relatively spared. These results confirm our previously published data. In this context, it is worth noting that in this report, ^{18}F-FAC was administered at tracer doses, but previously ^{14}C-gemcitabine was given in the presence of cold drug (40 mg/kg, in line with typical experimental dosing protocols for mice[21]). Therefore, the highly heterogenous distribution of gemcitabine/FAC does not seem to be a function of drug concentration, at least not over a therapeutically relevant range.

Regarding capecitabine, our starting hypothesis was that the wide distribution of radiolabel was likely due to slow cellular entrapment of capecitabine metabolites, giving the radiolabel greater time to diffuse through the tumor stroma. As capecitabine must undergo three enzymatic conversions prior to the first phosphorylation, it is intuitively reasonable that it would have relatively slow entrapment kinetics. However, a significant portion of capecitabine metabolites may be inactive, and thus the wide distribution of radiolabel may be meaningless. For the murine model we examined, 75% of the drug in the tumor is still in the form of either 5 FU or a 5 FU precursor. Previously we showed that directly injected [14]C-5 FU had a heterogeneous autoradiographic distribution more closely resembling gemcitabine and FAC than capecitabine,[9] and this supports our proposal that the additional delay required for activation of the capecitabine pro-drug improves its intra-tumoral distribution. These results are encouraging for capecitabine in pancreatic therapy, as it may have the ability to overcome the penetration barriers that are believed to hinder other chemotherapeutics. BxPC3 tumors show the same homogenous distribution

of capecitabine radiolabel but as this is accompanied by a more extensive metabolism of capecitabine, it is not clear whether the active species are also evenly distributed through the tumor. It would not be reasonable to expect the kinetics of capecitabine activation to be identical across all tumors, and if our understanding of the importance of the relative rates of drug activation, cellular entrapment, and diffusion is correct, then determining the rate of capecitabine activation in clinical pancreatic tumor samples will be an important next step.

Retrospective analysis of published clinical data indicates that the optimal treatment for pancreatic cancer is the FOLFIRINOX regime (5FU, leucovorin, irinotecan, and oxaliplatin), which displayed superior patient outcomes compared to both gemcitabine plus abraxane and gemcitabine plus capecitabine therapy regiments.[22] While these general observations are true collectively for cohorts, preclinical and emerging clinical data indicate that PDAC is heterogenous disease and therefore the optimal regime may be different for individual patients. For example, Yu and coworkers proposed gene expression profile-based therapy administration as an optimal strategy.[23] The only direct comparison between gemcitabine and capecitabine comes from studies where they are given in combination with radiotherapy; these trials suggest a modest benefit for capecitabine over gemcitabine.[24,25] As there is no PET tracer for capecitabine, it will not be possible to identify individuals with homogenous capecitabine uptake in their tumors; however, ^{18}F-FAC may be used to identify patients with unfavorable gemcitabine distributions, and this could aid in stratifying patient groups. The tracer has previously been administered to volunteers,[26] and is scheduled to be administered to pancreatic cancer patients at Memorial Sloan Kettering.

Finally, we would note that the general paradigm for pancreatic cancer is one of poor drug access. This is based on observations made with doxorubicin and gemcitabine.[4] While the present dataset would clearly be enhanced by the presence of markers of tumor response, particularly local response, such as γH2AX staining would supply, the results we obtained are still clearly different from what this paradigm predicts. This suggests that poor localization cannot be assumed for every agent, and the use of dual autoradiography allows different agents to be compared in this regard. Similar tumor distribution studies should be conducted for each component of pancreatic cancer chemotherapy.

DISCLOSURE

The authors declare that they have no conflicts of interest with the contents of this article.

AUTHORS' CONTRIBUTIONS

Russell, Fanchon, Molina, deStanchina, Pillarsetty, and Humm participated in the research design. Russell, Fanchon, Alwaseem, Pillarsetty, O'Donoghue, and Bahr conducted the experiments. Russell, Fanchon, and Alwaseem performed data analysis. Russell, Alwaseem, and Humm wrote or contributed to the writing of the manuscript.

ORCID

James Russell https://orcid.org/0000-0003-0827-1801

REFERENCES

1. Provenzano PP, Hingorani SR. Hyaluronan, fluid pressure, and stromal resistance in pancreas cancer. *Br J Cancer*. 2013;108(1):1-8. doi:10.1038/bjc.2012.569
2. Whatcott CJ, Diep CH, Jiang P, et al. Desmoplasia in primary tumors and metastatic lesions of pancreatic cancer. *Clin Cancer Res*. 2015;21(15):3561-3568. doi:10.1158/1078-0432.CCR-14-1051
3. Olive KP, Jacobetz MA, Davidson CJ, et al. Inhibition of Hedgehog signaling enhances delivery of chemotherapy in a mouse model of pancreatic cancer. *Science*. 2009;324(5933):1457-1461. doi:10.1126/science.1171362
4. Jacobetz MA, Chan DS, Neesse A, et al. Hyaluronan impairs vascular function and drug delivery in a mouse model of pancreatic cancer. *Gut*. 2013;62(1):112-120. doi:10.1136/gutjnl-2012-302529
5. Hakim N, Patel R, Devoe C, Saif MW. Why HALO 301 failed and implications for treatment of pancreatic cancer. *Pancreas*. 2019;3(1):e1-e4. doi:10.17140/POJ-3-e010
6. De Jesus-Acosta A, Sugar EA, O'Dwyer PJ, et al. Phase 2 study of vismodegib, a hedgehog inhibitor, combined with gemcitabine and nab-paclitaxel in patients with untreated metastatic pancreatic adenocarcinoma. *Br J Cancer*. 2020;122(4):498-505. doi:10.1038/s41416-019-0683-3
7. Dhani NC, Serra S, Pintilie M, et al. Analysis of the intra- and intertumoral heterogeneity of hypoxia in pancreatic cancer patients receiving the nitroimidazole tracer pimonidazole. *Br J Cancer*. 2015;113(6):864-871. doi:10.1038/bjc.2015.284
8. Metran-Nascente C, Yeung I, Vines DC, et al. Measurement of tumor hypoxia in patients with advanced pancreatic cancer based on 18F-fluoroazomyin arabinoside uptake. *J Nucl Med*. 2016;57(3):361-366. doi:10.2967/jnumed.115.167650
9. Fanchon LM, Russell J, Pillarsetty N, et al. Comparing the intra-tumoral distribution of Gemcitabine, 5-Fluorouracil, and Capecitabine in a murine model of pancreatic ductal adenocarcinoma. *PLoS One*. 2020;15(4):e0231745. doi:10.1371/journal.pone.0231745
10. Lamont EB, Schilsky RL. The oral fluoropyrimidines in cancer chemotherapy. *Clin Cancer Res*. 1999;5(9):2289-2296.
11. Peters GJ, van Groeningen CJ. Clinical relevance of biochemical modulation of 5-fluorouracil. *Ann Oncol*. 1991;2(7):469-480. doi:10.1093/oxfordjournals.annonc.a057994
12. Blanquicett C, Saif MW, Buchsbaum DJ, et al. Antitumor efficacy of capecitabine and celecoxib in irradiated and lead-shielded, contralateral human BxPC-3 pancreatic cancer xenografts: clinical implications of abscopal effects. *Clin Cancer Res*. 2005;11(24 Pt 1):8773-8781. doi:10.1158/1078-0432.Ccr-05-0627
13. Courtin A, Richards FM, Bapiro TE, et al. Anti-tumour efficacy of capecitabine in a genetically engineered mouse model of pancreatic cancer. *PLoS One*. 2013;8(6):e67330. doi:10.1371/journal.pone.0067330
14. Russell J, Pillarsetty N, Kramer RM, et al. In vitro and in vivo comparison of gemcitabine and the gemcitabine analog 1-(2'-deoxy-2'-fluoroarabinofuranosyl) cytosine (FAC) in human orthotopic and genetically modified mouse pancreatic cancer models. *Mol Imaging Biol*. 2017;19(6):885-892. doi:10.1007/s11307-017-1078-6
15. Gangangari KK, Humm JL, Larson SM, Pillarsetty NVK. TMSOTf assisted synthesis of 2'-deoxy-2'-[18F]fluoro-β-D-arabinofuranosylcytosine ([18F]FAC). *PLoS One*. 2018;13(5):e0196784. doi:10.1371/journal.pone.0196784
16. Soula M, Weber RA, Zilka O, et al. Metabolic determinants of cancer cell sensitivity to canonical ferroptosis inducers. *Nat Chem Biol*. 2020;16(12):1351-1360. doi:10.1038/s41589-020-0613-y
17. Harding SD, Sharman JL, Faccenda E, et al. The IUPHAR/BPS Guide to PHARMACOLOGY in 2018: updates and expansion to encompass the new guide to IMMUNOPHARMACOLOGY. *Nucleic Acids Res*. 2017;46(D1):D1091-D1106. doi:10.1093/nar/gkx1121

18. Alexander SPH, Kelly E, Mathie A, et al. THE CONCISE GUIDE TO PHARMACOLOGY 2019/20: introduction and other protein targets. *Br J Pharmacol.* 2019;176(Suppl 1):S1-S20. doi:10.1111/bph.14747

19. Lee JT, Campbell DO, Satyamurthy N, Czernin J, Radu CG. Stratification of nucleoside analog chemotherapy using 1-(2′-deoxy-2′-18F-fluoro-β-D-arabinofuranosyl)cytosine and 1-(2′-deoxy-2′-18F-fluoro-β-L-arabinofuranosyl)-5-methylcytosine PET. *J Nucl Med.* 2012;53(2):275-280. doi:10.2967/jnumed.111.090407

20. Russell J, Grkovski M, O'Donoghue IJ, et al. Predicting gemcitabine delivery by (18)F-FAC PET in murine models of pancreatic cancer. *J Nucl Med.* 2021;62(2):195-200. doi:10.2967/jnumed.120.246926

21. Sun JD, Liu Q, Ahluwalia D, et al. Efficacy and safety of the hypoxia-activated prodrug TH-302 in combination with gemcitabine and nab-paclitaxel in human tumor xenograft models of pancreatic cancer. *Cancer Biol Ther.* 2015;16(3):438-449. doi:10.1080/15384047.2014.1003005

22. Kharat A, Brendle M, Chhibber A, Chaiyakunapruk N, Biskupiak J. Comparative safety and efficacy of therapeutic options in resectable and advanced/metastatic pancreatic cancer: a systematic review and indirect comparison. *Oncol Res Treat.* 2021;44(9):476-484. doi:10.1159/000517409

23. Yu KH, Ricigliano M, McCarthy B, et al. Circulating tumor and invasive cell gene expression profile predicts treatment response and survival in pancreatic adenocarcinoma. *Cancers (Basel).* 2018;10(12):467. doi:10.3390/cancers10120467

24. Hurt CN, Falk S, Crosby T, et al. Long-term results and recurrence patterns from SCALOP: a phase II randomised trial of gemcitabine- or capecitabine-based chemoradiation for locally advanced pancreatic cancer. *Br J Cancer.* 2017;116(10):1264-1270. doi:10.1038/bjc.2017.95

25. Neibart SS, Mamidanna S, Chundury A, et al. Survival outcomes of patients with borderline resectable and resectable pancreatic adenocarcinoma treated with neoadjuvant short-course chemoradiotherapy with capecitabine-based vs. gemcitabine-based concurrent chemotherapy. *Int J Radiat Oncol Biol Phys.* 2021;111(3):e64. doi:10.1016/j.ijrobp.2021.07.414

26. Schwarzenberg J, Radu CG, Benz M, et al. Human biodistribution and radiation dosimetry of novel PET probes targeting the deoxyribonucleoside salvage pathway. *Eur J Nucl Med Mol Imaging.* 2011;38(4):11-21. doi:10.1007/s00259-010-1666-z